Preflare Nonthermal Emission Observed in Microwaves and Hard X-Rays

Ayumi Asai[1], Hiroshi Nakajima[1], Masumi Shimojo[1], Stephen M. White[2],
Hugh S. Hudson[3], and R. P. Lin[3]
[1]*Nobeyama Solar Radio Observatory, National Astronomical Observatory of Japan,*
Minamimaki, Minamisaku, Nagano, 384-1305, JAPAN
asai@nro.nao.ac.jp
[2]*Department of Astronomy, University of Maryland, College Park, MD20742, USA*
[3]*Space Science Laboratory, University of California, Berkeley, CA94720, USA*

(Received 2005 June 10; accepted)

Abstract

We present a detailed examination on the nonthermal emissions during the preflare phase of the X4.8 flare that occurred on 2002 July 23. The microwave (17 GHz and 34 GHz) data obtained with Nobeyama Radioheliograph, at Nobeyama Solar Radio Observatory and the hard X-ray data taken with *Reuven Ramaty High Energy Solar Spectroscopic Imager* obviously showed nonthermal features in the preflare phase. We also found a faint ejection associated with the flare in the EUV images taken with the *Transition Region and Coronal Explorer*. We discuss the temporal and spatial features of the nonthermal emissions in the preflare phase, and their relation with the ejection.

Key words: Sun: corona — Sun: flares — Sun: particle acceleration — Sun: radio radiation — Sun: X-rays, gamma rays

1. Introduction

Nonthermal emissions from accelerated particles are often observed in hard X-rays (HXRs), γ-rays, and microwaves at the beginning of a solar flare. These nonthermal emissions are associated with intense energy release processes, which characterize the "impulsive phase" of a flare. The particle acceleration mechanism has been one of the most important and the most difficult problems in solar physics (see reviews by, e.g. Aschwanden 2002). As Benz and Grigis (2003) and Lin & RHESSI Team (2003) reported recently, nonthermal emissions are associated with even a small energy release such as a microflare. However, it has been thought that the particle acceleration mechanism works efficiently only in the impulsive phase.

On the other hand, it is also interesting to study preflare activity, since this may hold the key for understanding how to trigger the catastrophic energy release of the flare. If we identify and understand the preflare signatures, we can anticipate the relevant physical processes of the flare itself. Preflare activity has thus often been studied (e.g. Simnett 1999). In the preflare stage we sometimes find flare-predictive phenomena, such as a gradual enhancement of soft X-ray (SXR) emission, rise of SXR plasmoids and/or Hα filaments, and so on. Even in the preflare stage of a solar flare, some energy release process is probably occurring at a low level, although the energy release is much milder.

However, we have not answered the question whether the energy release at this stage is a scaled-down version of the main flare, as in a microflare, or whether it is totally different. It is not widely accepted that nonthermal particles are present in significant numbers prior to the impulsive phase of a flare, rather it is common to speak of preflare heating implying thermal behaviour. Therefore, at least in terms of explosiveness of energy release, the impulsive phase seems to be distinguished from the preflare phase, and the reports on the nonthermal emissions during the preflare phases have been mostly negative. Fárník et al. (2003) reported the possibility of particle acceleration even in the preflare phase, although there still remain ambiguities.

Recentry, Holman et al. (2003) examined the HXRs features of the 2002 July 23 flare, and reported that the nonthermal energy even before the impulsive phase was quite large. Motivated by the work, we analyzed the flare, and found sufficient emissions both in HXRs and in microwaves that can be candidates for nonthermal emissions during the preflare phase. Especially, this is the first time of imaging observation of the preflare nonthermal emission in microwave. In order to derive information on the energy release in the preflare phase, we examined in detail the features of the emission sources spatially, temporally, and spectroscopically. In this paper we report the results of the investigations of the emissions in HXRs and in microwaves during the preflare phase. We also discuss the relation between the nonthermal emissions and other observed phenomena. In §2 we describe the observational data. In §3 we examine the detailed features of the nonthermal emissions, dividing the preflare phase into four sub-phases. In §4 we summarize our results and offer discussion.

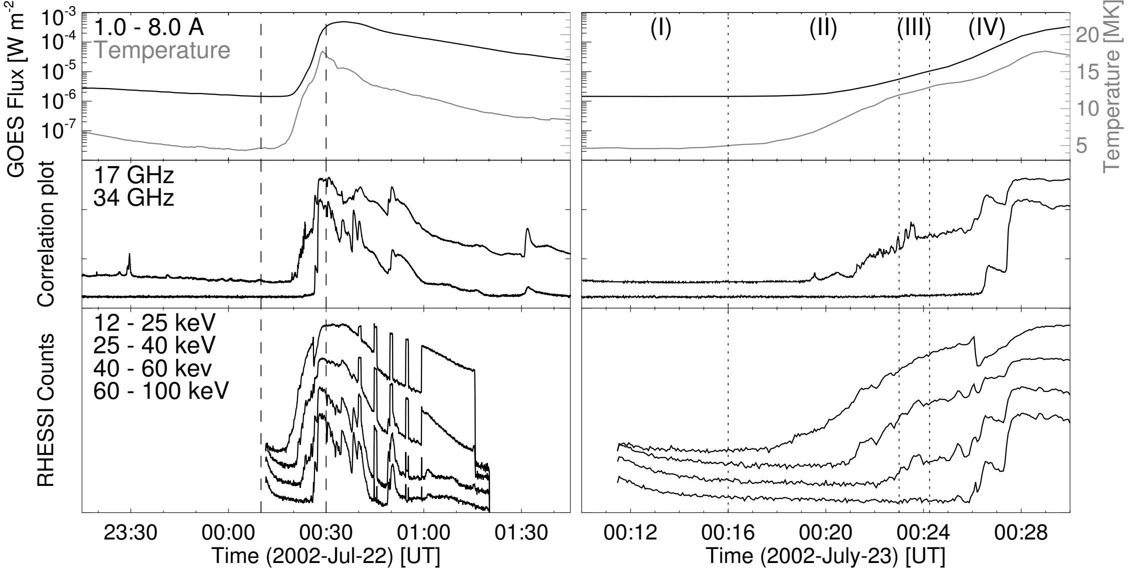

Fig. 1. *Left*: Light curves of the 2002 July 23 flare. From top to bottom: soft X-ray flux in the *GOES* 1.0 - 8.0 Å channel (*black*) and temperature derived from *GOES* fluxes (*gray*); radio correlation plot observed at 17 GHz and 34 GHz with NoRH (scaled arbitrary); hard X-ray count rate measured with *RHESSI* in four bands (12 - 25 keV, 25 - 40 keV, 40 - 60 keV, and 60 - 100 keV; scaled arbitrary). Two *dashed* vertical lines show the time range of the preflare phase. *Right*: Light curves of the preflare phase. Two *dotted* vertical lines divide the preflare phase into four sub-phases as numbered.

2. Observations and Data

The intense solar flare, which was X4.8 on the *GOES* scale, occurred in NOAA Active Region 10039 (S12°, E72°) at 00:18 UT, 2002 July 23. This flare showed many spectacular features (e.g. Lin et al. 2003) in HXR and γ-ray wavelengths obtained with the *Reuven Ramaty High Energy Solar Spectroscopic Imager* (*RHESSI*: Lin et al. 2002). This flare was also observed in microwaves with the Nobeyama Radioheliograph (NoRH: Nakajima et al. 1994) as reported by White et al. (2003). In this paper we focus on the nonthermal emissions in HXRs and in microwaves of the preflare phase, from about 23:00 UT, 2002 July 22 to about 00:30 UT, 2002 July 23. The left panel of Figure 1 shows the time profiles of the flare in SXRs, microwaves, and HXRs. The top two lines are the *GOES* 1.0 - 8.0 Å channel (*black* line) and the temperature profile (*gray* line), the middle ones are in NoRH 17 GHz and 34 GHz, and the bottom ones are the *RHESSI* time profiles in four energy ranges of 12 - 25 keV, 25 - 40 keV, 40 - 60 keV, and 60 - 100 keV. We divide the preflare phase into four sub-phases, and examine each phase in more detail in the following sections. The right panels of Figure 1 show the expanded light curves of the preflare phase of the flare (from 00:10 UT to 00:30 UT, 2002 July 23), which corresponds to the time between the dashed lines in the left panel. The time ranges of the four sub-phases are numbered at the top of the right panel of Figure 1.

NoRH observes the Sun in two frequencies, 17 GHz and 34 GHz, which allows us to derive a spectral index α ($F_\nu \propto \nu^\alpha$; F_ν is the flux at frequency ν) with a temporal resolution of 1 s. The spatial resolutions (FWHMs) of NoRH data are $14''$ for 17 GHz and $7''$ for 34 GHz. We synthesized the HXR images obtained with *RHESSI* by using grids 4 - 8 which gives the spatial resolution (FWHM) of about $12''$. We integrated over 20 seconds to synthesize each image in this paper. We also measured the temperature and the emission measure of the thermal plasma in the corona by using the ratios of the two of *GOES* channels. We plotted the time profiles of the temperature derived from *GOES* in the top panels of Figure 1. EUV images of the flare were obtained with the *Transition Region and Coronal Explorer* (*TRACE*; Handy et al. 1999; Schrijver et al. 1999). We used 195 Å images, in which the Fe XII line formed at $\sim$ 1 MK is normally dominant. The pixel size of the CCD is $1\farcs0$, and the temporal resolution is about 9 s.

3. Results

3.1. Phase I; before the flare

This phase corresponds to the time from about 23:30 UT, 2002 July 22 to 00:16 UT, 2002 July 23. Figure 2 shows the images of the flare for each phase. The left panels show the *TRACE* 195 Å images overlaid with the contour images of the NoRH 34 GHz (*red*), the *RHESSI* 25 - 40 keV (*yellow*), and the 40 - 60 keV (*blue*, only in the bottom panel), respectively. The right panels show the maps of NoRH α index overlaid with the *RHESSI* 12 - 25 keV intensity (*white*). We can see a large loop-like bright region in the NoRH image (White et al. 2003). We measured the spectral index α of the emission source, and found that it is about 0 (within from -0.4 to 0.6). Therefore, the optically-thin (free-free) thermal emission is dominant for the source. Moreover, the polarization of the sources is no more than 10 %, which eliminates the

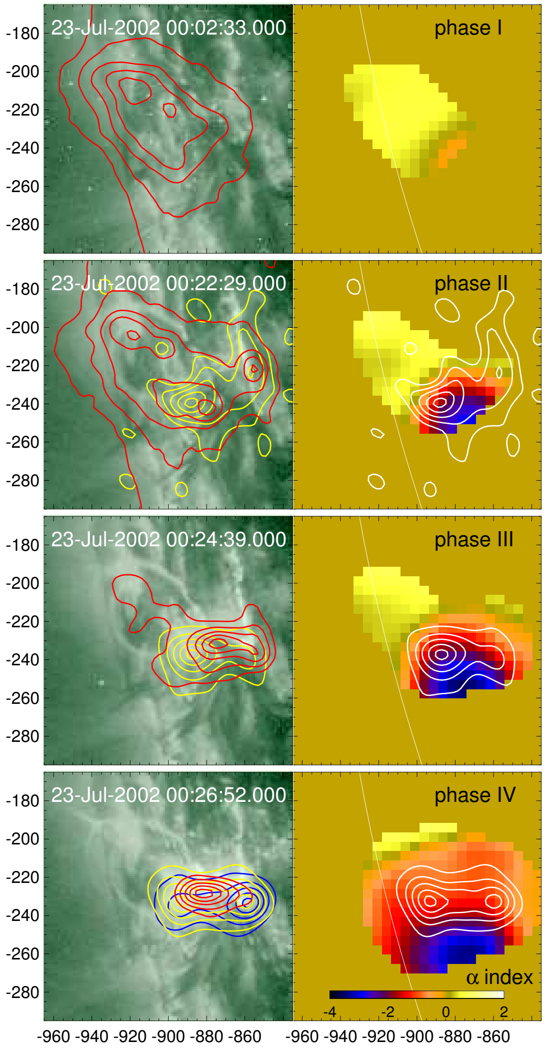

Fig. 2. Images of the flare for each phase. Solar north is up, and west is to the right. The left panels show the EUV images taken with *TRACE* 195 Å. The contours show the NoRH 34 GHz brightness temperature (*red*), the *RHESSI* 25 - 40 keV intensity (*yellow*), and the 40 - 60 keV intensity (*blue*, only in the bottom panel), respectively. The right panels show the maps of NoRH α index overlaid with the *RHESSI* 12 - 25 keV intensity (*white*). The 34 GHz contours are 15, 30, 50, 70, and 90 % of the peak intensity. Contours for the *RHESSI* HXR images are at 20, 40, 60, 80, and 95 % of the peak intensity.

possibility of the emission from the gyroresonance near sunspot umbrae. To confirm this, we also estimated the microwave fluxes in 17 and in 34 GHz from the temperature and the emission measure which were derived from *GOES*, and found that the estimated fluxes was almost the same as the observed ones. We defined the emission from the background corona as the average emission between 20:30 UT and 21:10 UT on 2002 July 22.

The *GOES* temperature shows the existence of hot plasma even in this phase of about 5 MK (see the top panels of Figure 1). This could be related to a small flare which occurred at 22:00 UT in the same active region, although we could not confirm due to the lack of image data for the small event. It was at a time before NoRH started observations, and *RHESSI* was unavailable due to the SAA and the night. Although *TRACE* was observing the region, we cannot see any active phenomena at the time. This is presumably because the large structure is too hot to be observed in the EUV range. In any case we cannot see any signs of triggering the flare in this phase.

3.2. Phase II; preflare phase

This phase includes the first flare emissions (from 00:16 UT to 00:23 UT). We can see some thermal emission features and also clear signatures of nonthermal emission. This phase is the most important one for this paper.

First, we summarize the features of the time profiles. The *GOES* temperature rapidly increases from about 4.5 MK at 00:15 UT to above 10 MK at 00:22 UT. At the same time, the *RHESSI* count rate in 12 - 25 keV increases as shown in Figure 1. Such HXR brightenings in lower energy bands, associated with a hotter *GOES* source, are often observed in a preflare phase, and the emissions are thought to be thermal. Holman et al. (2003) performed a spectroscopic analysis of the flare with *RHESSI* data, and reported that the thermal component of the region has high temperature up to 20 - 30 MK. After some short delay, from 00:18 UT the NoRH 17 GHz emission starts to rise, and the temporal evolution resembles the *RHESSI* 25 - 40 keV light curve. The NoRH 34 GHz emission and the *RHESSI* 40 - 60 keV count rate start to rise at 00:22 UT almost simultaneously.

Here we summarize the spatial features of the emission sources. The panels in the second row from the top of Figure 2 show the images of the phase taken at 00:22:30 UT. In the *TRACE* images, we can see that a large two-ribbon structure (White et al. 2003) brightens from 00:20 UT. The brightening of the ribbons implies that a larger structure rather than the core of the flare destabilizes in this phase. In Figure 3 we present the enlarged images which show the spatial features. The *TRACE* EUV images in the left and the middle panels were taken a few minutes after this phase. We can see a diffuse loop-like structure that is identified as Fe XXIV emission from 20 MK plasma, as is often observed in *TRACE* 195 Å images during flares. A new microwave source appears above the flare ribbons at (-878, -243) arcsec heliocentric. This site corresponds to the post flare loops, which become visible in the later phase in the *TRACE* images

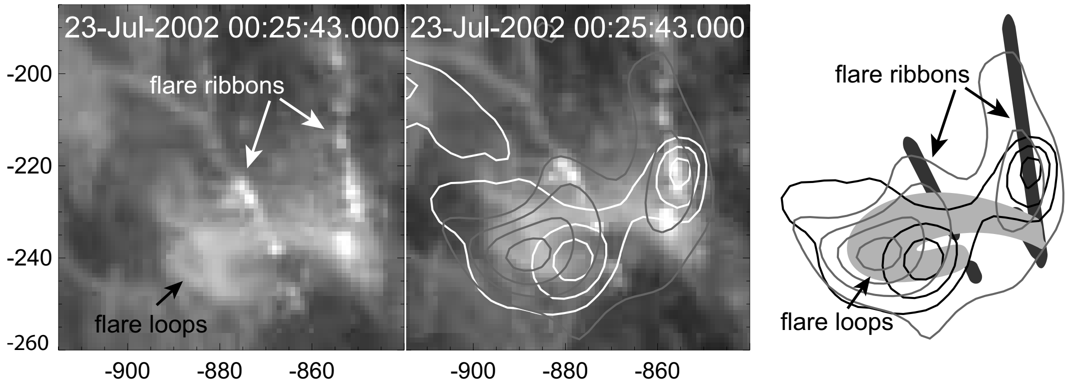

Fig. 3. Spatial distribution of the emission sources. Solar north is up, and west is to the right. The left and the middle panels show EUV images taken with *TRACE* 195 Å. The contours in the middle and the right panels show the NoRH 34 GHz brightness temperature (*white* in the middle and *black* in the right panel), and the *RHESSI* 25 - 40 keV intensity (*gray*), respectively. The right panel also shows the positions of the flare ribbons (*dark gray* regions) and the flare loops (*light gray*).

and which connect the flare ribbons. The α index is about -3.0, which implies that this source is emitting nonthermal-gyrosynchrotron radiation. The index is quite small and shows a steep (soft) power-law spectrum. An HXR source also appears at this site, although apparently slightly higher (-890, -240) than the microwave emission source. Figure 3 shows the HXR source to be at the top of the diffuse *TRACE* loop. The HXR source is visible in both 12 - 25 keV and 25 - 40 keV bands. These sources could resemble to the "loop-top" HXR source (Masuda et al. 1994). On the other hand, we can also see footpoint sources which are located on the *TRACE* flare ribbons mentioned above both in the microwave (34 GHz) and in the HXRs (12 - 25, 25 - 40 keV). The energy release probably occurs in the corona, some part of which is deposited at the footpoints to produce the EUV brightenings. The HXR emissions from the flare ribbon are thought to be generated by thick-target emission by nonthermal electrons. This is evidence for the existence of the nonthermal particles in this phase.

3.3. Phase III; ejection

Next, we focus on the small microwave burst and the faint EUV ejection which occurred at about 00:23:30 UT. In Figure 4 we show the relationship between the timing of the EUV ejection and the nonthermal microwave emission. The arrows indicate the time when the ejection started. The projected speed of the ejection on the time slice image is roughly about 250 km s^{-1}. A halo coronal mass ejection (CME) associated with the flare was also observed with Large Angle Spectrometric Coronagraph (LASCO) on board the *Solar and Heliospheric Observatory* (*SOHO*: see the *SOHO* LASCO CME online catalog[1]; Yashiro et al. 2004). The combination of ejections and HXR bursts has been observed in impulsive flares (Kano 1994; Hudson, Acton & Freeland 1996; Ohyama & Shibata 1997), and is consistent with the so-called "plasmoid-induced reconnection model" (Shibata 1999). The plasmoid ejections correspond in detail with nonthermal emissions, and CME acceleration may also show this pattern (e.g. Zhang et al. 2001).

The NoRH 34 GHz source moved northward slightly (-875,-230), and showed a loop like structure. This loop structure corresponds to the most intense post-flare loop which appeared later in the *TRACE* 195 Å images. The HXR *RHESSI* 12 - 25 keV and 25 - 40 keV emissions still appear at the top of the NoRH loop. Although the source positions moved northward as to the 34 GHz emission, they cannot be identified because of limitations of the spatial resolution.

3.4. Phase IV; impulsive phase

This phase corresponds to the time after the *TRACE* ejection and before the start of the impulsive phase (from 00:24 UT to 00:27 UT). Roughly speaking, the physical features are the same as in the impulsive phase, as Krucker, Hurford & Lin (2003) reported. The positions of the emission sources do not change so much from the previous phase, III. The HXR coronal sources ascend slightly as the flare progresses. The 34 GHz emission comes to localize gradually on the upper section of the loop. As a notable result, we can see an HXR loop-top source even in 40 - 60 keV as shown in the bottom left panel of Figure 2. In this phase, the α index increases slightly (becomes harder) to about -1.5.

4. Discussion and Summary

In this paper, we examined in detail the nonthermal emissions in the preflare phase spatially, temporally, and spectroscopically. We also examined the relation between the nonthermal emissions and other observed phenomena. We identified a faint EUV ejection in the *TRACE* data which was associated with a nonthermal microwave burst, just before the fast energy release process occurs in the impulsive phase. In the phase before the ejection, we found observational evidence of both thermal and nonthermal emissions in the corona above the flare ribbon structure.

---

[1] See http://cdaw.gsfc.nasa.gov/CME_list/.

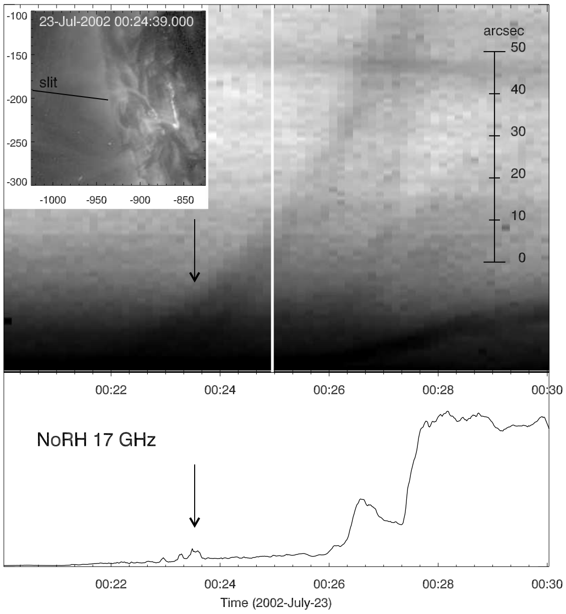

Fig. 4. *Top left*: an EUV image of the flare observed with *TRACE*. The *black* solid line illustrates the position of the slit line. *Top right*: time-sequenced EUV (195 Å) image (time slice image) obtained with *TRACE* along the slit line. The horizontal and the vertical axes are time (UT), and the space along the slit, respectively. *Bottom*: microwave (17 GHz) light curve obtained with NoRH.

Under the standard reconnection model, the current sheet reduces its thickness in the preflare phase (Magara & Shibata 1999), which leads to the fast magnetic reconnection and the violent energy release in the impulsive phase. This process is associated with the slow reconnection and/or the low-level energy release, and leads to heating the coronal plasma as often observed. Our results, on the other hand, indicate that the process also releases enough energy with the right conditions to accelerate particles to nonthermal energies. This suggests that energy release mechanism in the preflare phase of a typical flare may be accompanied by particle acceleration, although it is much milder than that in the impulsive phase and therefore difficult to detect in flares smaller than this event.

We first acknowledge an anonymous referee for his/her useful comments and suggestions. We wish to thank Drs. G. D. Holman, L. Sui for fruitful discussions and their helpful comments. We made extensive use of *TRACE* and *RHESSI* Data Center.

References

Aschwanden, M. J. 2002, Space Sci. Rev., 101, 1
Benz, A. O. & Grigis, P. C. 2003, Adv. Space Res., 32, 1035
Fárník, K., Hudson, H. S., Karlický, M., Kosugi, T. 2003, A&A, 399, 1159
Handy, B. N., et al. 1999, Sol. Phys., 187, 229
Holman, G. D., Sui, L., Schwartz, R. A. & Emslie, A. G. 2003, ApJL, 595, L97
Hudson, H. S., Acton, L. W., & Freeland, S. L. 1996, ApJ, 470, 629
Kano, R. 1994, in X-Ray Solar Physics from Yohkoh, ed. Y. Uchida, T. Watanabe, K. Shibata, & H. S. Hudson (Tokyo: Universal Academy Press), 273
Krucker, S., Hurford, G. J. & Lin, R. P. 2003, ApJL, 595, L103
Lin, R. P., et al. 2002, Sol. Phys., 210, 3
Lin, R. P., et al. 2003, ApJL, 595, L69
Lin, R. P. & RHESSI Team 2003, Adv. Space Res., 32, 1001
Magara, T. & Shibata, K. 1999, ApJ, 514, 456
Masuda, S., Kosugi, T., Hara, H., Tsuneta, S. & Ogawara, Y. 1994, Nature, 371, 495
Nakajima, H., et al. 1994, in Proc. of the IEEE, 82, 705
Ohyama, M. & Shibata, K. 1997, PASJ, 49, 249
Schrijver, C. J. et al. 1999, Sol. Phys., 187, 261
Shibata, K., Masuda, S., Shimojo, M., Hara, H., Yokoyama, T., Tsuneta, S., Kosugi, T. & Ogawara, Y. 1995, ApJL, 451, L83
Shibata, K. 1999, Ap&SS, 264, 129
Simnett, G. M. 1999, in The Many Faces of the Sun, ed. K. T. Strong, J. L. R. Saba, B. M. Haisch & J. T. Schmelz (New York: Springer), 201
White, S. M., Krucker, S., Shibasaki, K., Yokoyama, T., Shimojo, M., Kundu, M. R. 2003, ApJL, 595, L111
Yashiro, S., Gopalswamy, N., Michalek, G., St. Cyr, O. C., Plunkett, S. P., Rich, N. B., and Howard R. A. 2004, J. Geophys. Res., 109, A07105
Zhang, J., Dere, K. P., Howard, R. A., Kundu, M. R., & White, S. M. 2001, ApJ, 559, 452